A Semi-Automatic Method to Identify Vertebral End Plate Lesions (Schmorl's nodes).

Nicolas Newell, Caroline A. Grant, Maree T. Izatt, J. Paige Little, Mark J. Pearcy, Clayton J. Adam

Paediatric Spine Research Group, Queensland University of Technology and Mater Health Services Brisbane Ltd, Queensland, Australia

Corresponding author:

Dr Nicolas Newell

Postdoctoral Research Fellow

School of Chemistry, Physics and

Mechanical Engineering, Queensland

University of Technology,

O-Block, Level 4, Room 413,

Gardens Point Campus,

GPO Box 2434,

Brisbane 4001,

Australia.

Tel: +61 7 3138 2423

E-mail: nic.newell@qut.edu.au

Abstract

Background Context: There are differences in definitions of end plate lesions (EPLs), often referred to as Schmorl's nodes, that may, to some extent, account for the large range of reported prevalence (3.8 - 76%).

Purpose: To develop a technique to measure the size, prevalence and location of EPLs in a consistent manner.

Study Design/Setting: This study proposed a method using a detection algorithm which was applied to five adolescent females (average age 15.1 years, range 13.0 to 19.2 years) with idiopathic scoliosis (average major Cobb angle 60°, range 55 to 67°).

Methods: Existing low-dose, computed tomography scans were segmented semi-automatically to extract 3D morphology of each vertebral endplate. Any remaining attachments to the posterior elements of adjacent vertebrae or endplates were then manually sectioned. An automatic algorithm was used to determine the presence and position of EPLs.

Results: EPLs were identified in 15 of the 170 (8.8%) endplates analysed with an average depth of 3.1mm. 11/15 of the EPLs were seen in the lumbar spine. The algorithm was found to be most sensitive to changes in the minimum EPL gradient at the edges of the EPL.

Conclusions: This study describes an imaging analysis technique for consistent measurement of the prevalence, location and size of EPLs. The technique can be used to analyse large populations without observer errors in EPL definitions.

Keywords

End plate lesion, Schmorl's node, Scoliosis

1. Introduction

There is general consensus that end plate lesions (EPLs), often referred to as Schmorl's nodes, can be defined as a herniation of intervertebral disc tissue into the vertebral body [1–5]. However, more specific definitions tend to differ. Constraints include: indentations located centrally on the endplate [6], delineation by a thin sclerotic boundary [6], minimum size (distance from most anterior to most posterior edge of the EPL measured on sagittal images) [3] or the exclusion of smooth concave curvatures that have their centre located at the posterior portion of the endplate (otherwise known as Cupid's bows) [3–5] since these are not considered to be pathological [7, 8].

These differences may, to some extent, account for the large range of reported prevalence (3.8 - 76%). Hilton et al. [9] analysed 50 slab radiographs (cadaveric specimens, sliced sagittally into slabs that are individually radiographed) of thoracolumbar specimens (T9-S1) aged 13 - 96 years, finding that 76% had EPLs at one or more levels; also looking at slab radiographs (100 cadaveric thoracolumbar specimens, mean age 68 years, range 43 - 93 years) Pfirrmann and Resnick [4] found 58% of their specimens had at least one EPL; analysing 372 contrast enhanced magnetic resonance images (MRIs) of the thoracic and lumbar spine in subjects with a mean age of 53 years, Stäbler et al. [3] reported that EPLs were present in 38% of the subjects; and Sonne-Holm et al. [6] reported that at least one EPL was present in 3.8% of a series of 4151 plain, lateral radiographs of lumbar spines in subjects aged 22 - 93 years (median 63 years).

The large discrepancies in reported prevalence could also be explained by the different imaging modalities used to observe EPLs. It has been suggested that observation of EPLs is more difficult on plain radiographs in comparison to MRI and slab radiographs [4, 10], and that CT scans may provide a more precise method of observing EPLs [6].

A number of studies have attempted to measure the location and size of EPLs as well as their prevalence. They are generally found at the thoracolumbar junction either centrally or posteriorly on the endplate, but rarely anteriorly [2, 4–6, 9]. Two studies have found that EPLs are more common in the endplates on the caudal side of the vertebra in comparison to the cranial [4, 9], but others have found no difference [2, 6]. It is common for EPLs to be found at multiple levels in the same patient and there is a tendency for successive vertebral surfaces to be affected with nodes of similar shape and position [2, 4, 6, 9]. Pfirrmann and Resnick [4] found that EPLs had a mean diameter of 6 mm (range 2-15 mm), a mean height of 3.3 mm (range 1-9 mm) and a mean volume of 86 mm^3 (range 2-923 mm^3). Stäbler et al. [3] reported a slightly larger mean diameter of 8.2 mm (range 4-20 mm), however this could be accounted for by the fact that they excluded any EPLs with a diameter less than 3 mm, unfortunately depth and volume were not reported in this study.

Both the aetiology and pathogenesis of EPLs is uncertain [6, 9]. It has been postulated that they are either inert developmental or congenital herniations into weak areas of the end plate or that they are due to trauma, infection, osteoporosis, malignancy or various bone diseases [1, 6]. It has also been suggested that they form at locations that have been weakened due to incomplete resorption of the notochord or anomalies in the avascularisation of the

intervertebral disc during development [2, 3]. The interaction between EPLs and disc degeneration remains unclear and controversial [10]; a number of studies have suggested that there is a link [5, 9, 11], while others have not been able to confirm this correlation [4, 12]. A recent study comparing patients with lumbar symptoms to a control group found that EPLs are more likely to be found in patients with pain in the lumbar spine (EPLs were found in 9% of the control group and 19% of the symptomatic group) [12], although the relationship of EPLs to low back pain is still debated [6]. Similarly, the relationship between EPLs and race, gender, age, body weight or exposure to heavy manual labour is uncertain [6].

EPLs have been observed in idiopathic scoliosis patients but to the authors' knowledge, their prevalence, location and size have not previously been reported. Buttermann and Mullin [13] analysed MRIs of 60 consecutive paediatric and adult idiopathic scoliosis patients who had progressed to surgical treatment and found a correlation between EPLs and pain in paediatric scoliosis patients but not in adult scoliosis patients. A pilot investigation has also suggested that EPLs may potentially be a primary disturbance of growth plates that leads to the onset of scoliosis [14].

Given the abovementioned variability in definition of EPLs, the aim of this study was to develop an image analysis technique for consistent measurement of the prevalence, location and size of EPLs. The wide range of reported prevalence of EPLs highlights the importance of a well-defined, repeatable and reliable method to identify them. A semi-automatic approach will eliminate inter-observer differences in EPL definitions and facilitate rapid comparison of multiple data sets. It is important that the vertebral tilt and rotation seen in idiopathic scoliosis

patients is considered when detecting EPLs and therefore we describe the tool development and application using a series of pre-operative CT scans of idiopathic scoliosis patients.

2. Materials and methods

Imaging

Low-dose, computed tomography (CT) scans, covering vertebral levels C7-S1 were taken of patients with adolescent idiopathic scoliosis (AIS) using a Toshiba Aquilion Multi scanner (Toshiba Medical Systems Corp., Tokyo, Japan). The scan used a 100 kV, 50 mA source with a 6 mm pitch and a 1 second rotation time, producing raw images with 0.6 x 0.6 x 1.0 mm voxels. It is estimated that this scanning protocol exposed the paediatric patients to a radiation dose of 3.7 ± 0.74 mSv (estimate ± uncertainty) [15]. This is higher than the combined dose for full length postero-anterior and lateral standing radiographs (approximately 1.0 mSv), but substantially lower than a typical adult chest CT scan (approximately 8 mSv [16]). At the time of data collection, a single supine preoperative CT scan was part of the clinical assessment process for AIS patients undergoing single anterior rod instrumentation via the thoracoscopic approach to allow safer screw sizing and positioning [17]. Subsequently, we have obtained approval from our institution's Human Research Ethics Committee to use the historical dataset of clinical CT scans for research purposes.

Segmentation

The CT scans were segmented (Amira® software, Version 5.1.1, VSG - Visualization Sciences Group, Burlington, MA, USA) using a semi-automatic approach. Initially, the geometry of each vertebra was automatically segmented using a threshold of 300 Hounsfield units (HU). A

number of threshold values were compared across our dataset and this value was found to be the most accurate in defining bone edges. A threshold of 300 HU lies within the range used by authors of a number of other studies (225 – 325 HU) [18–21]. Following the automatic segmentation, any attachments between posterior elements of adjacent vertebrae were manually sectioned, and, if necessary, the endplates were also manually segmented to ensure that there was separation between each level. The resulting surface geometry for each vertebra was imported into Geomagic® XOS™ (Version 4.1.0.0, Raindrop Geomagic Inc., Research Triangle Park, NC, USA). The inter- and intra-observer error in the manual segmentation was investigated through multiple segmentations of the L1-L4 levels of one spine. Intra-observer error was investigated by the same observer (CG) performing the segmentation of the same spine section twice, approximately one week apart and inter-observer error was investigated by a second observer (NN) using the same segmentation technique on the same spine section. The 95% limits of agreement, as proposed by Bland and Altman [22, 23], were calculated for the EPL prevalence and depth. This method involves finding the differences between measurements, then calculating the mean and the standard deviation (SD) of those differences. The 95% limits of agreement were then defined as the mean difference ± 1.96×SD. Thus, 95% of the differences between measurements are expected to lie between these two reported limits.

Using Geomagic® XOS™ the effects of noise were reduced by using the built-in smoothing command. A value of 0.4 mm was settled upon for the maximum allowable deviation as this was sufficient smoothing to eliminate any noise but not too large that surface features were lost. To investigate the sensitivity of this smoothing on the output of the analysis, calculations

were also made on endplates that had been smoothed with a maximum allowable deviation of both 0.2 and 0.6 mm. After smoothing, point clouds of the cranial and caudal end plates were exported for later analysis.

Endplate co-ordinate system

For consistency in reporting lesion locations, a local coordinate system was assigned to each endplate, defined through manual identification of relevant landmarks. The endplate transverse plane was defined by selecting 3 points (shown in Figure 1): A) a point 5 mm from the middle of the junction between the left pedicle and the vertebral body along the axis of the pedicle; B) a point 5 mm from the middle of the junction between the right pedicle and the vertebral body along the axis of the pedicle; and C) a point 5 mm from the intersection between the anterior edge of the vertebral body and a line parallel to line A→B (along a line perpendicular to line A→B that passes through the anterior intersection).

<< Insert Figure 1 >>

The endplate sagittal plane was defined using a similar method to that described by Aaro and Dahlborn [24] to estimate vertebral rotation. This method involves selecting two points; the endplate centroid and the posterior junction of the two laminae of the vertebral arch. Vrtovec et al. [25] compared Aaro and Dahlborn's method of measuring vertebral rotation against four other manual techniques [26–28], finding that the Aaro and Dahlborn method was the most reproducible and reliable. For this study, the endplate centroid was calculated using a similar method to that previously described by Little et al. [29] and shown in Figure 2: a rectangle was drawn on the transverse plane that passed through two points at the posterior inflection points on the anulus boundary (points 1 and 2), the anterior anulus boundary (point 3) and the

lateral points on the anulus boundary (points 4 and 5). The geometric centre of this rectangle was used as the endplate centroid.

<< Insert Figure 2 >>

An orthogonal left-handed coordinate system was created on the transverse plane at the endplate centroid where the sagittal plane was defined by a vector passing between the endplate centroid and the posterior junction of the two laminae of the vertebral arch. The positive x direction was anterior, the positive y direction was to the patient's right and the positive z direction was superior.

Automatic EPL detection algorithm

Following the manual identification of landmarks used to define the endplate local coordinate systems, an automatic algorithm, written in MATLAB (Version R2012a, The MathWorks Inc., Natick, MA, USA), was used to determine the presence, location and size of EPLs. The scattered point cloud data of the endplate, now in the local coordinate system, was imported and interpolated using the *griddata* function in MATLAB such that the surface points were on a regular grid, with grid lines 0.5 mm apart, running anterior/posterior and left/right (Figure 3a).

Troughs were identified along each grid line (Figure 3b). Start and end points of potential troughs, were defined as locations where both the preceding and succeeding point along the grid line were lower (local maxima) and similarly, trough points were defined as locations where the preceding and succeeding point were higher (local minima).

<< Insert Figure 3 >>

The largest trough along each grid line was identified by calculating the area of the triangle made between each set of start, trough and end points. The trough with the largest area was selected as the potential EPL location for that grid line (the blue trough would be selected from the gridline depicted in Figure 3b). Potential EPL locations were then discarded if certain conditions were not met. Four conditions, determined through preliminary measurements of EPLs from the CT scans and influenced by literature values, were determined.

First, that the depth of the trough (taken as the distance between the z-coordinate of the trough point and an average of the z coordinates of the start and end points) was greater than 2 mm. Pfirrmann and Resnick [4] quoted a mean depth of 3.3 mm with a range of 1-9 mm and since the voxels of the CT scans analysed here are 0.6 x 0.6 x 1 mm in dimension (x, y and z respectively) a minimum depth of 2 mm was used to ensure that the EPL was at least 2 voxels deep.

Second, that the trough point was greater than 5 mm from the edge of the vertebral body so that small undulations on short gridlines at the edge of the endplate were not mistaken for EPLs. The edge of the vertebral body was identified by searching each grid line in both directions for the first point that was more than 0.1 mm higher than the previous point.

Third, to ensure that Cupid's bows were not included in this definition of an EPL, the gradient between either the start-trough or trough-end points was required to be greater than 0.2 mm/mm, such that a 2 mm deep trough (depth threshold defined previously) will only be

included as an EPL if it is at the centre of a trough with a diameter less than 20 mm (the maximum of the range of EPL diameters measured by Stabler et al. [3]).

Fourth, to reduce the probability of anomalies being detected on one grid line, a second potential EPL location was required to be detected in an area bounded by a 2 x 2 x 2 mm cube centred around the first EPL location.

Potential EPL locations were detected on grid lines along both the sagittal and coronal planes, and in the case that more than one potential EPL location was found, the deepest was selected as the maximum EPL location. In the cases where none of the potential EPL locations met the conditions it was assumed that no EPL was present.

EPLs were categorised according to their location relative to the local coordinate system in the transverse plane. To allow comparison of EPL locations between endplates, the EPL coordinates in the local endplate coordinate system were normalised to be a percentage of the distance between the endplate centroid and the furthest of either the most anterior or most posterior points of the vertebral body in the sagittal plane. Two methods were used to group the EPL locations. First, each vertebral end plate was divided into 4 quarters; anterior, posterior, left lateral and right lateral (Figure 4a). Second, the location of the EPLs relative to the centre were grouped into 5 concentric zones around the endplate centroid, 20, 40, 60, 80 and >80% of the distance between the endplate centroid and the furthest of either the most anterior or most posterior points of the vertebral body in the sagittal plane (Figure 4b).

<< Insert Figure 4 >>

The locations of any EPLs were also displayed in Amira® software alongside the original CT scan to confirm that the automatically detected EPLs were at locations that could also be identified upon visual inspection.

In order to gain an understanding of how sensitive the calculated prevalence is to the condition values a simple sensitivity study was undertaken, where the EPL condition values were adjusted by ±10 and ±20% from their baseline values described previously and all of the endplates were analysed. The baseline and adjusted values are shown in Table 1. Each value was adjusted individually resulting in 16 complete analyses for each spine, plus the baseline analysis.

<< Insert Table 1 >>

3. Results

Prevalence and Depth

The endplates from the spines of five adolescent females (average age 15.1 years, range 13.0 to 19.2 years) with idiopathic scoliosis (average major Cobb angle 60°, range 55 to 67°) were analysed. EPLs were identified in 15 of the 170 (8.8%) endplates (Note, 12x2=24 thoracic endplates and 5x2=10 lumbar endplates in each patient), with eight on the caudal side of the vertebral body in question and seven on the cranial side. Eleven of the 15 EPLs were seen in the lumbar spine, and of the four in the thoracic spine, all were at or inferior to T11. The average EPL depth was 3.1 mm (range 2.1 to 5.3 mm) and deeper EPLs were found in the lumbar spine in comparison to the thoracic (mean depths of 3.6 and 2.5 mm, respectively). An example of a sagittal and coronal slice through a potential EPL location is shown in Figure 5a

and b, respectively. An example of the 3D surface before smoothing obtained using a threshold of 300 HU can be seen in Figure 5c and the location of the EPL on that surface is represented by the yellow ball shown in Figure 5d.

<< Insert Figure 5 >>

The number of EPLs found in each endplate zone can be seen in Figure 6. The posterior zone had the largest number of EPLs (7/15) while just one EPL was observed in the anterior zone and this was very close to the centre (within 20% of the distance between the endplate centroid and the furthest of either the most anterior or most posterior points of the vertebral body in the sagittal plane). No EPLs were observed further than 68% away from the endplate centroid.

<< Insert Figure 6 >>

Sensitivity of EPL detection condition values

The detection algorithm was most sensitive to changes in the minimum gradient (Figure 7d) with an extra 12 EPLs detected when the minimum gradient was decreased from 0.2 to 0.16 (-20%) and six fewer EPLs detected when the minimum gradient was increased from 0.2 to 0.24 (+20%). However, smaller changes in the minimum gradient (±10% of the baseline value) resulted in just two greater or two fewer EPL being detected in the 170 endplates analysed. By comparison the detection algorithm was relatively insensitive to changes in the minimum depth (Figure 7a), minimum distance from the edge of the endplate (Figure 7b) and the length of the sides of the cube within which a second potential EPL was required to be detected (Figure 7c).

<< Insert Figure 7 >>

Inter- and intra- observer segmentation error

The L1-L4 section from the spine of patient #5 was chosen for the inter- and intra-observer error analysis since the detection algorithm had identified EPLs on every endplate apart from the L3 cranial endplate. There was 100% agreement in the prevalence of EPLs when comparing the two segmentations performed by CG one week apart or when NN repeated the comparison and therefore the 95% limits of agreement in prevalence are not reported. The inter-observer difference in EPL depth was 0.03mm ± 0.17mm (mean difference ± 95% limit of agreement), and 0.04mm ± 0.14mm for the intra-observer difference. The fact that the mean differences for both the inter- and intra-observer variances were not significantly different from zero, suggests that no order bias existed.

Sensitivity of segmentation threshold and smoothing

Adjusting the maximum allowable deviation and the Hounsfield unit threshold for the segmentation did not have an effect on the prevalence of EPLs. However, the smoothing of the surface had some effect on the calculated depth, with differences of up to 6.37 and 9.43% (0.33 and 0.4 mm) when the maximum allowable deviation in smoothing was decreased from 0.4 to 0.2 mm and increased from 0.4 to 0.6 mm, respectively (Table 2). The EPL depth measurements were more sensitive to changes in the automatic segmentation threshold with differences of up to 38.03% (1.78 mm) seen in EPL depth when the threshold was increased from 300 to 400 HU. Finally, differences of up to 18.84% (0.76 mm) were seen in the depth when the automatic segmentation threshold was decreased from 300 to 200 HU.

<< Insert Table 2 >>

4. Discussion

This study describes an imaging analysis technique for consistent measurement of the prevalence, location and size of EPLs. The semi-automatic approach eliminates inter-observer differences in EPL definitions allowing a well-defined, repeatable and reliable method to identify EPLs.

Since the aim of this study was to primarily develop a reproducible and accurate measurement technique, a relatively small number of endplates have been analysed. However, the prevalence of EPLs found here (8.8%) was within the lower bounds of previously reported prevalence (3.8 - 76%) [3, 4, 6, 9]. The average depth of EPLs found in this study (3.1 mm) was similar to that reported by Pfirrman and Resnick [4] (3.3 mm). In agreement with the

findings of a number of other studies [2, 4–6, 9], the majority of the EPLs were found posteriorly with just one of the 15 EPLs in the anterior zone. It has been postulated that EPLs may be associated with the weakening of the endplate due to abnormalities in the regression of the notochord during development. Since 93% of the EPLs detected in this cohort were within a 60% radius from the endplate centroid it may be postulated that this data supports this theory, however, further analysis of a larger dataset would be required before this can be confirmed.

A possible limitation of this method for identifying EPLs is that it is reliant on the segmentation of CT scans, which when automatic thresholding does not result in separate endplates, requires manual segmentation. Generally, we found manual segmentation was more frequently required in upper thoracic in comparison to lower thoracic or lumbar vertebrae. The fact that the intra- and inter-observer variability in EPL depth measurements represents only 2.8 – 3.5% of the depth, within the size of a voxel (0.5mm), and that there was 100% inter- and intra-observer agreement in the prevalence demonstrates the precision of this method. In addition, the majority of EPLs were detected in the lumbar region, where manual segmentation was rarely required. EPL identification was sensitive to the minimum gradient condition value, where adjustments of just 20% resulted in a further 12 EPLs being identified. To some extent this does not come as a surprise since the large range of reported prevalence demonstrates the sensitive nature of identifying EPLs. A strength of the semi-automatic approach taken here is that the condition values are clearly defined and the sensitivity to these values can be investigated. Thus far, this algorithm has only been applied to surfaces extracted from CT scans. Due to the radiation dose associated with CT scans, their use is diminishing in

modern medicine in favour of other assessment tools. This also limits the possibility of using this technique to analyse the endplates of healthy populations for research, unless scans have been ordered for an unrelated purpose. Future investigation is therefore required to determine whether the algorithm is able to detect EPLs using surfaces extracted from MRI and other imaging modalities.

5. Conclusions

A well-defined, repeatable and reliable method to measure EPL prevalence, location and size has been developed that can be used to analyse large populations without observer errors in EPL definitions. Although the method developed here was assessed by the identification of EPLs on vertebrae of five adolescent idiopathic scoliosis patients, it has the potential to also be used to identify EPLs in both healthy adolescent and adult populations.

6. References

1. Schmorl G, Junghanns H: *The Human Spine in Health and Disease*. 2nd Americ. New York: Grune & Stratton; 1971:504.

2. Saluja G, Fitzpatrick K, Bruce M, Cross J: **Schmorl's nodes (intravertebral herniations of intervertebral disc tissue) in two historic British populations**. *J Anat* 1986, **145**:87–96.

3. Stabler A, Weiss M, Gartner C, Brossmann J, Reiser F: **MR Imaging of Enhancing Intraosseous Disk Herniation (Schmorl's Nodes)**. *Am J Roentgenol* 1997, **168**:933–938.

4. Pfirrmann CWA, Resnick D: **Schmorl Nodes of the Thoracic and Lumbar Spine : Radiographic-Pathologic Study of Prevalence, Characterization, and Correlation with**

Degenerative Changes of 1,650 Spinal Levels in 100 Cadavers. *Radiology* 2001, **219**:368–74.

5. Wu H-TH, Morrison WB, Schweitzer ME: **Edematous Schmorl's nodes on thoracolumbar MR imaging: characteristic patterns and changes over time.** *Skeletal Radiol* 2006, **35**:212–9.

6. Sonne-Holm S, Jacobsen S, Rovsing H, Monrad H: **The epidemiology of Schmorl's nodes and their correlation to radiographic degeneration in 4,151 subjects.** *Eur spine J* 2013, **22**:1907–12.

7. Dietz GW, Christensen EE: **Normal "Cupid's Bow" Contour of the Lower Lumbar Vertebrae 1**. 1976:577–579.

8. Ramirez H, Navarro JE, Bennett WF: **"Cupid's bow" contour of the lumbar vertebral endplates detected by computed tomography.** *J Comput Assist Tomogr* 1984, **8**:121–4.

9. Hilton RC, Ball J, Benn RT: **Vertebral end-plate lesions (Schmorl's nodes) in the dorsolumbar spine.** *Ann Rheum Dis* 1976, **35**:127–132.

10. Benneker LM, Heini PF, Anderson SE, Alini M, Ito K: **Correlation of radiographic and MRI parameters to morphological and biochemical assessment of intervertebral disc degeneration.** *Eur spine J* 2005, **14**:27–35.

11. Wang Y, Videman T, Battié MC: **ISSLS prize winner: Lumbar vertebral endplate lesions: associations with disc degeneration and back pain history.** *Spine (Phila Pa 1976)* 2012, **37**:1490–6.

12. Hamanishi C, Kawabata T, Yosii T, Tanaka S: **Schmorl's nodes on magnetic resonance imaging. Their incidence and clinical relevance.** *Spine (Phila Pa 1976)* 1994, **19**:450–3.

13. Buttermann GR, Mullin WJ: **Pain and disability correlated with disc degeneration via magnetic resonance imaging in scoliosis patients.** *Eur spine J* 2008, **17**:240–9.

14. Day G, Frawley K, Phillips G, McPhee IB, Labrom R, Askin G, Mueller P: **The vertebral body growth plate in scoliosis: a primary disturbance of growth?** *Scoliosis* 2008, **3**.

15. Schick D: *Computed Tomography Radiation Doses for Pediatric Scoliosis Scans. Internal Report Commissioned by Pediatric Spine Research Group from Queensland Health Biomedical Technology Services*. 2004.

16. Valentin J. **Managing patient dose in computed tomography.** ICRP publication; 87; *Annals of the ICRP, v3, no.4:* International Commission of Radiological Protection.; 2001.

17. Kamimura M, Kinoshita T, Itoh H, Yuzawa Y, Takahashi J, Hirabayashi H, Nakamura I: **Preoperative CT Examination for Accurate and Safe Anterior Spinal Instrumentation Surgery with Endoscopic Approach.** *J Spinal Disord Tech* 2002, **15**:47–51.

18. Sylvestre P-L, Villemure I, Aubin C-E: **Finite element modeling of the growth plate in a detailed spine model.** *Med Biol Eng Comput* 2007, **45**:977–88.

19. Giambini H, Khosla S, Nassr A, Zhao C, An K-N: **Longitudinal changes in lumbar bone mineral density distribution may increase the risk of wedge fractures.** *Clin Biomech (Bristol, Avon)* 2013, **28**:10–4.

20. Parenteau CS, Wang NC, Zhang P, Caird MS, Wang SC: **Quantification of pediatric and adult cervical vertebra-anatomical characteristics by age and gender for automotive application.** *Traffic Inj Prev* 2014, **15**:572–82.

21. Gill S, Abolmaesumi P, Fichtinger G, Boisvert J, Pichora D, Borshneck D, Mousavi P: **Biomechanically constrained groupwise ultrasound to CT registration of the lumbar spine.** *Med Image Anal* 2012, **16**:662–74.

22. Bland J, Altman D: **Applying the right statistics: analyses of measurement studies**. *Ultrasound Obstet Gynecol* 2003, **22**:85-93.

23. Bland J, Altman D: **Statistical methods for assessing agreement between two methods of clinical measurement**. *Lancet* 1986, **327**:307–310.

24. Aaro S, Dahlborn M: **Estimation of vertebral rotation and the spinal and rib cage deformity in scoliosis by computer tomography.** *Spine (Phila Pa 1976)* 1981, **6**:460.

25. Vrtovec T, Vengust R, Likar B, Pernus F: **Analysis of four manual and a computerized method for measuring axial vertebral rotation in computed tomography images.** *Spine (Phila Pa 1976)* 2010, **35**:E535–41.

26. Ho E, Upadhyay S, Chan DF: **New methods of measuring vertebral rotation from computed tomographic scans: an intraobserver and interobserver study on girls with scoliosis**. *Spine (Phila Pa 1976)* 1993, **18**:1173.

27. Göçen S, Havitçioğlu H, Alici E: **A new method to measure vertebral rotation from CT scans**. *Eur Spine J* 1999, **8**:261.

28. Krismer M, Sterzinger W, Haid C, Frischhut B, Bauer R: **Axial rotation measurement of scoliotic vertebrae by means of computed tomography scans**. *Spine (Phila Pa 1976)* 1996, **21**:576.

29. Little JP, Pearcy MJ, Pettet GJ: **Parametric equations to represent the profile of the human intervertebral disc in the transverse plane.** *Med Biol Eng Comput* 2007, **45**:939–45.

7. Figure Legends

Figure 1 – Landmarks identified in order to define the endplate transverse plane. Point A is 5 mm from the middle of the junction between the left pedicle and the vertebral body along the axis of the pedicle. Point B is 5 mm from the middle of the junction between the right pedicle and the vertebral body along the axis of the pedicle and Point C is 5 mm from the intersection between the anterior edge of the vertebral body and a line parallel to line A→B, along a line perpendicular to line A→B that passes through the intersection. Units are in mm.

Figure 2 – Method to identify the endplate centroid based on a method previously proposed by Little et al. [29]. A rectangle was drawn on the transverse plane that passed through two points at the posterior inflection points on the anulus boundary (points 1 and 2), the anterior anulus boundary (point 3) and the lateral points on the anulus boundary (points 4 and 5). The geometric centre of this rectangle was used as the endplate centroid. The origin of the left handed orthogonal system is shown at the geometric centre.

Figure 3 – (a) Diagram showing a 3D representation of the grid over the surface of an endplate, the thick black line highlights the gridline that is shown in 2D in (b). On this gridline, 3 potential trough locations were detected; the start, trough and end points of each of these potential locations are circled and joined together with red, blue and green lines, respectively.

Figure 4 – Zones of the vertebral endplate used to group EPL locations. The percentages in (b) refers to the percent of the distance between the furthest of either the most anterior or most superior points of the vertebral body in the sagittal plane.

Figure 5 – (a) Sagittal and (b) coronal slices through the same L2 vertebral body showing potential EPLs on both the upper and lower endplate. (c) The 3D surface obtained from segmenting this vertebra using a threshold of 300 HU and (d) the location of the EPL detected on the upper endplate of this vertebra represented by a yellow ball. Note that the surfaces have not been smoothed in (c) or (d).

Figure 6 – Locations of the EPLs relative to the geometric centre of each endplate. The concentric rings represent zones 20, 40, 60 and 80% of the distance between the furthest of either the most anterior or most superior points of the vertebral body in the sagittal plane.

Figure 7 – Sensitivity of the EPL detection condition values on the number of EPLs detected relative to the number of EPLs detected when the baseline EPL detection condition values were used. Positive numbers on the y-axis represent additional EPLs that were detected when (a) the minimum depth condition value, (b) the minimum distance from the edge of the endplate value, (c) the minimum length of the sides of the cube within which a second potential EPL was required to be detected and (d) the minimum gradient condition value was adjusted by the percentages shown on the x-axis. Similarly, negative y-axis values represent fewer EPLs that were detected.

8. Tables

Table 1 – Baseline and adjusted EPL detection conditions for the sensitivity study.

Variable	-20%	-10%	Baseline Value	+10%	+20%
Minimum depth (mm)	1.6	1.8	2	2.2	2.4
Minimum distance from edge of endplate (mm)	4	4.5	5	5.5	6
Size of cube within which a second EPL is required to be detected (mm)	1.6	1.8	2	2.2	2.4
Minimum gradient between either the start and trough or trough and end points of an EPL (mm/mm)	0.16	0.18	0.2	0.22	0.24

Table 2 – Sensitivity in the depth measurements of the EPL associated with the maximum allowable deviation in smoothing and the Hounsfield unit threshold used for the segmentation.

		Maximum allowable deviation during smoothing		Hounsfield unit (HU) threshold	
Level	Cranial/ Caudal endplate	% difference when decreased from 0.4 to 0.2 mm	% difference when increased from 0.4 to 0.6 mm	% difference when decreased from 300 to 200 HU	% difference when increased from 300 to 400 HU
L1	Cranial	-5.64	2.22	-8.77	12.53
	Caudal	-6.37	7.02	-15.59	2.24
L2	Cranial	-5.26	9.43	-10.79	-38.03
	Caudal	-2.85	2.55	-8.59	7.99
L3	Cranial	-3.50	0.75	3.91	8.64
	Caudal	n/a	n/a	n/a	n/a
L4	Cranial	-1.23	5.49	-18.37	28.73
	Caudal	3.47	0.51	-2.86	-4.85
Greatest difference (%)		**-6.37**	**9.43**	**-18.37**	**-38.03**

Figure 1.

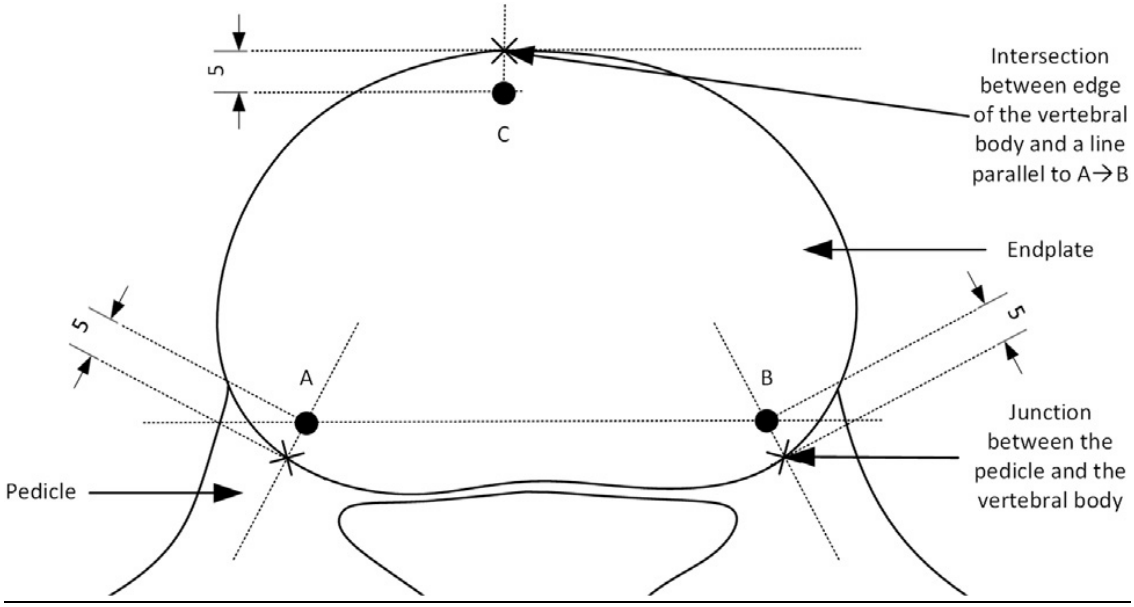

Figure 2.

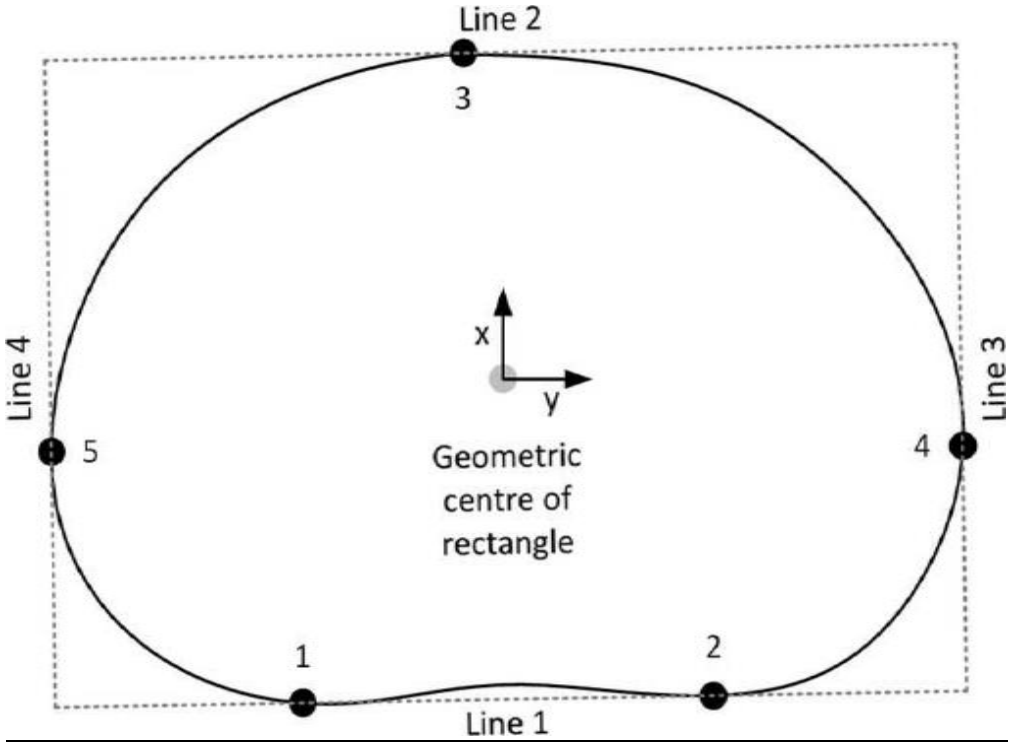

Figure 3.

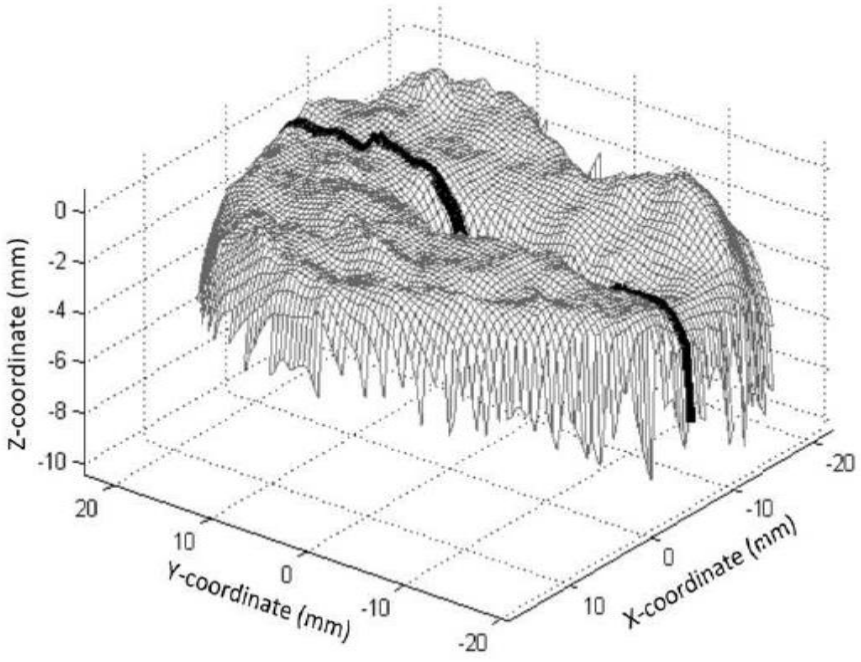
Z-coordinate (mm)
0
-2
-4
-6
-8
-10
20
10
0
-10
-20
Y-coordinate (mm)
-20
-10
0
10
X-coordinate (mm)

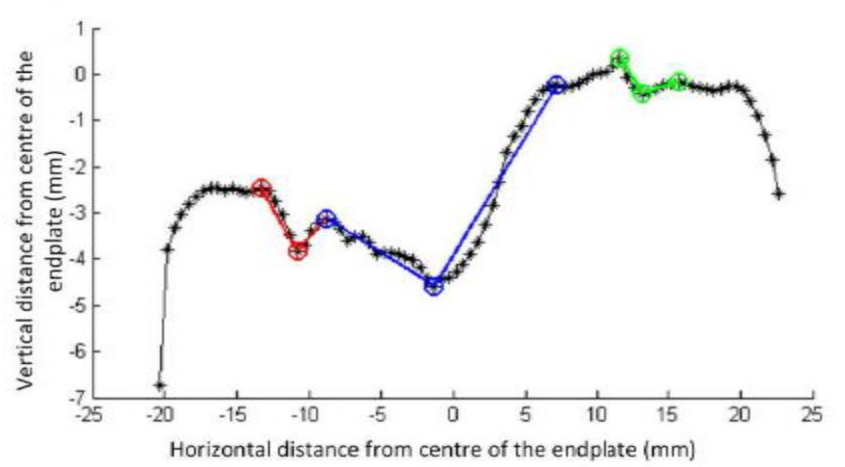
Vertical distance from centre of the endplate (mm)
1
0
-1
-2
-3
-4
-5
-6
-7
-25
-20
-15
-10
-5
0
5
10
15
20
25
Horizontal distance from centre of the endplate (mm)

Figure 4.

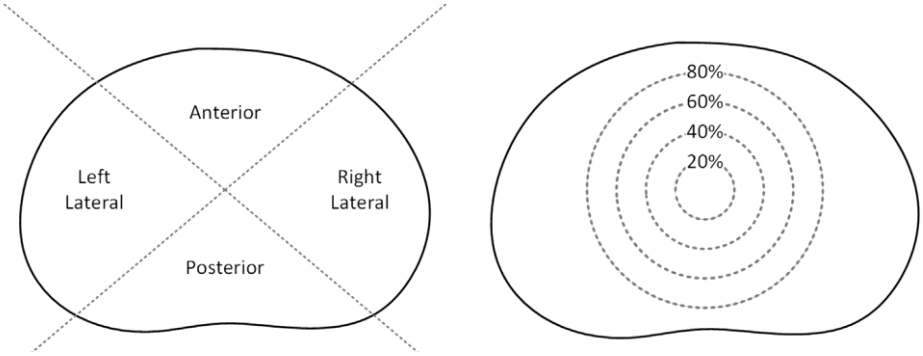

Figure 5.

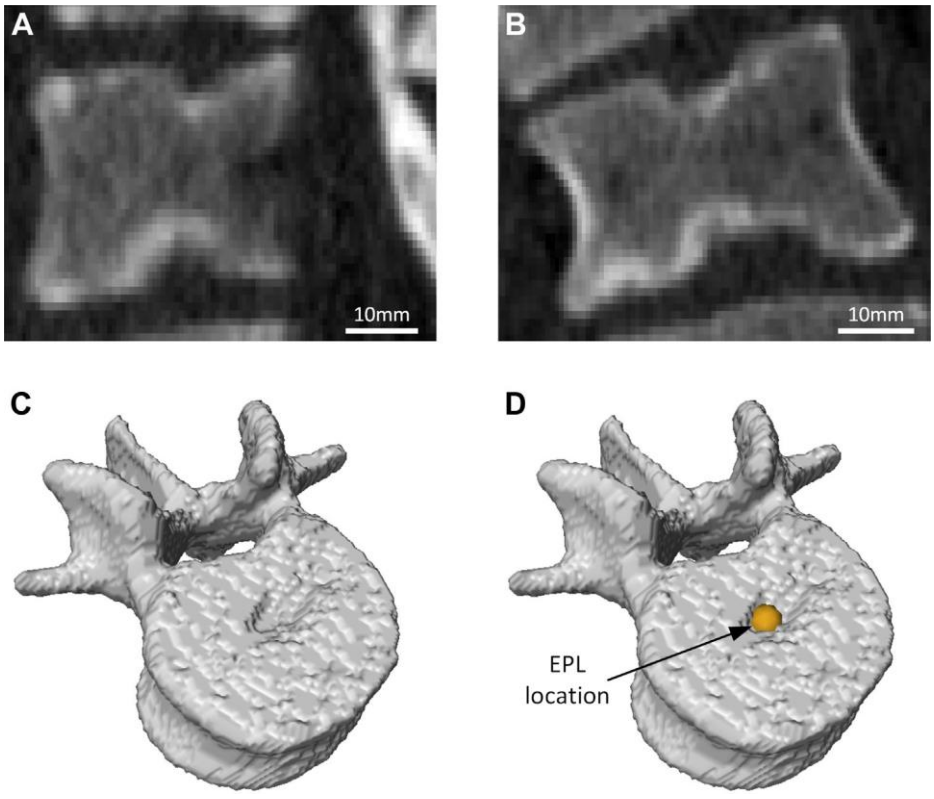

Figure 6.

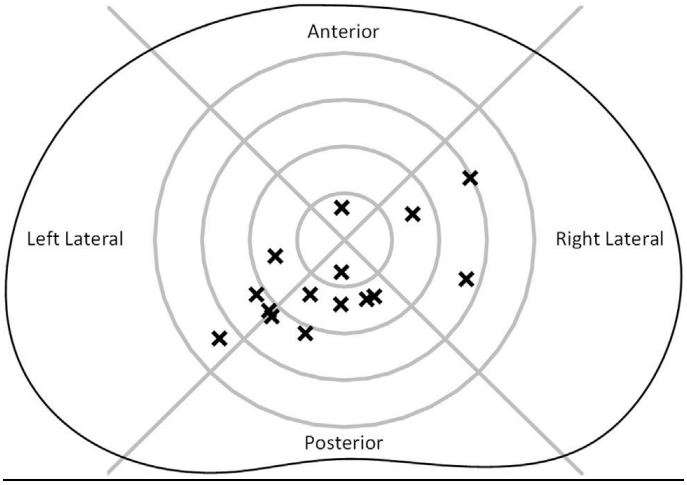

Figure 7.